Investigating Atomic and Molecular Systems in Ultra-strong Magnetic Fields Using Neural Network Variational Monte Carlo

Author

CID 02222285 Tianyue Yang[1]
CID 02267384 Sahil Khandelwal[1]

Supervised by

Professor William Matthew Colwyn Foulkes[1]

Assessed by

Professor Dimitri Vvedensky[1]

[1]: *Department of Physics, Imperial College London, SW7 2AZ, United Kingdom*

Abstract

Matters in ultra-strong magnetic fields, such as those found in neutron stars and white dwarfs, exhibit unique quantum behaviours, necessitating advanced computational methods for accurate modelling. In this study, Neural Network Variational Monte Carlo (NN-VMC) was employed to investigate the ground-state and binding energies of the hydrogen molecule across magnetic field strengths ranging from $B = 0.001$ to 1.0 atomic units ($1.0\,\text{a.u.} \approx 2.35 \times 10^5\,\text{T}$), considering both singlet and triplet spin configurations. For the first time, nuclear motion was incorporated into simulations in strong magnetic fields without relying on the Born-Oppenheimer approximation, enabling the exploration of coupling effects between nuclear dynamics and magnetic fields.

The results demonstrated that NN-VMC achieved superior accuracy compared to conventional Configuration Interaction (CI) methods, with energy values up to 0.1% lower for singlet states, leading to improved predictions of binding energies. Quantum-nucleus simulations revealed deviations from fixed-nucleus predictions, with bond lengths differing by approximately $0.5a_0$ for singlet states and up to $2.0a_0$ for triplet states, underscoring the limitations of the Born-Oppenheimer approximation in strong magnetic fields. A benchmark study involving a two-electron system in a harmonic potential showed reasonable agreement between NN-VMC and semi-analytical solutions. Despite challenges in resolving binding energies for triplet states, influenced by Van der Waals interactions, this study demonstrates the robustness and versatility of NN-VMC in modelling quantum systems under extreme conditions.

Contents

Chapter 1 Introduction 2

1.1 Quantum Mechanics with Magnetic Field 2
1.1.1 Background 2
1.1.2 The Hamiltonian 2
1.2 Born-Oppenheimer Approximation 3
1.3 Aims 4
1.3.1 Existing Approaches 4
1.3.2 Ground State Energy and Binding Energy 5
1.3.3 Comparison of Bond Lengths 5
1.3.4 Validating the Method Against Analytical Models 5

Chapter 2 Methodology 6

2.1 Neural Network Variational Monte Carlo 6
2.1.1 Variational Monte Carlo 6
2.1.2 Neural Network Ansatz 7
2.1.3 Energies and Observables 8
2.1.4 Implementation and Validation 8
2.2 Analytical Models 8
2.2.1 Two-Electron System in a Harmonic Potential 8
2.2.2 N-Boltzmannons with Quadratic Interactions 9

Chapter 3 Results & Discussion 10

3.1 Bond Lengths and Energies 10
3.1.1 Results 10
3.1.2 Discussion 11
3.2 Two-Electron System in Harmonic Potential 13
3.2.1 Results 13
3.2.2 Discussion 13

Chapter 4 Conclusion & Acknowledgement 14

4.1 Conclusion 14
4.2 Acknowledgement 14

Chapter A Appendix 15

A.1 Cyclotrons, Landau Levels and Fock-Darwin States 15
A.2 Finite Difference Method 16
A.3 N - Boltzmannons with Quadratic Interactions 16
A.4 Metropolis-Hasting Algorithm 18
A.5 Hyperparameters for FermiNet 18

Introduction

1.1 Quantum Mechanics with Magnetic Field

1.1.1 Background

Magnetic fields ranging from 1 to 100 MT, characteristic of neutron stars, represent a regime far beyond what can be replicated on Earth. [1] At these strengths, the Born-Oppenheimer approximation may fail, requiring the quantum mechanical treatment of all particles, including protons and neutrons. This greatly increases the complexity of the problem due to the interplay of Coulomb interactions and the large number of interacting particles.

Such systems are analytically unsolvable, requiring numerical methods. However, the challenges posed by extreme magnetic fields made these computations increasingly demanding as particle numbers grew. To the author's knowledge, this work was the first to apply FermiNet in such extreme magnetic fields. To ensure its accuracy, this study also benchmarked FermiNet's results against semi-analytical solutions.

1.1.2 The Hamiltonian

Magnetic fields have been studied in quantum systems for a long time, both theoretically and computationally. For an N-particle system, the total Hamiltonian is written as

$$\hat{H}_{\text{total}} = \sum_{i=1}^{N} \frac{1}{2m_i} \left(\hat{\vec{p}}_i - q_i \vec{A} \right)^2 + \sum_{i<j} \frac{q_i q_j}{4\pi\varepsilon_0 |r_i - r_j|}, \tag{1.1}$$

where $\hat{\vec{p}}_i = -i\hbar\vec{\nabla}_i$, q_i is the charge, $\vec{A}$ is the magnetic vector potential defined as $\vec{B} = \vec{\nabla} \times \vec{A}$ and i is the particle index. Since $\vec{A}$ is a gauge field, a specific gauge must be chosen to perform computations. The standard practice for numerical studies has been to use the symmetric Coulomb gauge:

$$\vec{A} = \frac{1}{2}\vec{B} \times \vec{r}. \tag{1.2}$$

As $\vec{A}$ becomes complicated for position-dependent or time-dependent $\vec{B}$, it is usually more practical to consider only a uniform magnetic field in the z direction (B_z) in a Cartesian coordinate system. In this case, $\vec{A}$ simplifies to

$$\vec{A} = \frac{1}{2} B_z \begin{pmatrix} -y \\ x \\ 0 \end{pmatrix}. \tag{1.3}$$

In the strong magnetic field regime, the impact of the linear Zeeman effect becomes signifi-

cant, requiring the inclusion of a term depending on the total particle spin:

$$\hat{H}_{\text{total}} = \sum_{i=1}^{N} \frac{1}{2m_i} \left(\hat{\vec{p}}_i - q_i \vec{A} \right)^2 + \sum_{i \neq j} \frac{q_i q_j}{4\pi\varepsilon_0 |r_i - r_j|} + \frac{\mu_B B_z}{\hbar} \left(g_s S_z + g_l L_z \right), \tag{1.4}$$

where g_s (g_l) is the dimensionless gyromagnetic factor, S_z is the sum of particle spins in the z direction, and $L_z = -i\hbar \left(x \frac{\partial}{\partial y} - y \frac{\partial}{\partial x} \right)$ is the z component of the orbital angular momentum. Throughout this project, the following values for the gyromagnetic factors are used:

$$g_s \approx 2.0023193, \quad g_l = 1. \tag{1.5}$$

To simplify the problem and enhance the stability of numerical calculations, the Hartree Atomic Unit (referred to as the atomic unit in this report) is used. This unit is defined such that:

$$\hbar = 4\pi\varepsilon_0 = e = m_e = 1. \tag{1.6}$$

The distance unit naturally becomes the Bohr radius of the hydrogen atom (a_0). In this unit, the Bohr magneton μ_B becomes:

$$\mu_B = \frac{e\hbar}{2m_e} = \frac{1}{2}. \tag{1.7}$$

Since the regime of magnetic field strengths of interest is from 10^3 to 10^6 Tesla, it is preferable to work with a larger unit. The atomic unit of magnetic field B is defined such that the cyclotron radius $\rho_0 = \sqrt{\frac{\hbar}{eB}}$, which serves as the characteristic length scale of magnetic systems (See A.1 for details), is equal to the Bohr radius a_0:

$$\frac{\hbar}{eB} = a_0^2, \tag{1.8}$$

which leads to:

$$B_{\text{a.u.}} = \frac{\hbar}{e a_0^2} \equiv 1 \text{ a.u.} \approx 2.35 \times 10^5 \text{ T}. \tag{1.9}$$

The Hamiltonian of magnetic systems in this set of units is written as:

$$\hat{H}_{\text{total}} = \sum_{i=1}^{N} \frac{1}{2m_i} \left(\hat{\vec{p}}_i - q_i \vec{A} \right)^2 + \sum_{i \neq j} \frac{q_i q_j}{|r_i - r_j|} + \frac{1}{2} B_z \left(g_s S_z + L_z \right), \tag{1.10}$$

where the particle mass m_i and charge q_i are expressed in units of m_e and e, respectively.

1.2 Born-Oppenheimer Approximation

The Born-Oppenheimer approximation assumes that nuclei possess large masses such that they move on a much longer time scale. This assumption separates the total time-independent Schrödinger equation into electronic and nuclear equations. For scalar potentials that depend only on position vectors, the electronic equation can be written as:

$$\left[-\sum_i \frac{\hbar^2}{2m_e} \nabla_i^2 + \sum_{i,I} U_{\text{e-n}}(r_i; r_I) + \sum_{i \neq j} U_{\text{e-e}}(r_i, r_j) \right] \psi = \epsilon \psi, \tag{1.11}$$

where $U_{\text{e-e}}$ and $U_{\text{e-n}}$ represent the electron-electron and electron-nuclear interactions, respectively. Here, $\epsilon(r_I)$ is the electronic energy, which depends parametrically on the nuclear positions r_I, and I indexes the nuclei. The corresponding nuclear Schrödinger equation becomes:

$$\left[-\sum_I \frac{\hbar^2}{2m_I}\nabla_I + \epsilon(r_I)\right]\chi(r_I) = E\chi(r_I), \tag{1.12}$$

where E is the total energy and χ represents the nuclear wavefunction. For most chemical systems, this approximation works well because electrons move much faster than nuclei, contributing only a near-constant energy shift. However, this may not apply to systems under the influence of a strong magnetic field.

This is due to the fact that the coupling between nuclear motion and the magnetic field becomes non-negligible in the strong-field regime. For a homonuclear diatomic molecule, the full Hamiltonian can be rearranged as:

$$\begin{aligned}\hat{H}_{\text{elec}} = \frac{1}{2M}K^2 - \frac{e}{M}\vec{K}\cdot\left(\vec{B}\times\sum_i \vec{r}_i\right) + \sum_i \frac{1}{2m}\left(\hat{\vec{p}}_i - \frac{e}{2}\vec{B}\times\vec{r}_i\right)^2 \\ + \frac{2}{M_0}\left(\hat{\vec{P}} + \frac{eZ}{4}\vec{B}\times\vec{R}\right)^2 + \frac{1}{2M_0}\left(\sum_i \hat{\vec{p}}_i + \frac{e}{2}\vec{B}\times\sum_i \vec{r}_i\right)^2 + V\left(\vec{r}_i;\vec{R}\right),\end{aligned} \tag{1.13}$$

where M is the total mass, m is the electronic mass, M_0 is the nuclear mass, $\vec{r}_i$ are the positions of electrons relative to the centre of mass of the nuclei, $\vec{R}$ is the relative vector of the two nuclei, $\hat{\vec{P}}$ is the canonical momentum of the nuclei with respect to their centre of mass, and $\vec{K}$ is a constant vector. If one performs the standard process of nucleus-electron separation, the equation becomes:

$$\left[\frac{2}{M_0}\left(\hat{\vec{P}} + \frac{eZ}{4}\vec{B}\times\vec{R}\right)^2 + \epsilon_{\text{elec}}(\vec{K};\vec{R}) - E\right]\chi_m(\vec{R}) = \sum_n \Lambda_{mn}\chi_n(\vec{R}), \tag{1.14}$$

where ϵ_{elec} is the electronic energy. The right-hand side of this equation contains the off-diagonal non-adiabatic terms, which are ignored under the Born-Oppenheimer approximation, potentially leading to significant deviations from the real scenario. Please refer to [2] and [3] for more details. Deriving analytical solutions for these equations is extremely difficult, and, to the best of the author's knowledge, no existing research claims to yield exact solutions [4].

With neural network variational Monte Carlo, we can study the effect of the coupling between nuclear motion and the magnetic field for the first time.

1.3 Aims

1.3.1 Existing Approaches

To the best of the author's knowledge, existing studies primarily adopt three major approaches: Hartree-Fock (HF), Configuration Interaction (CI), and Variational Monte Carlo (VMC). The HF method, based on the self-consistent field procedure, by definition, cannot account for the correlation energy among particles. This limitation is a significant drawback of the HF approach, as correlation energy is central to this field of study. CI and VMC, on the

other hand, are relatively accurate because they can fully capture correlation effects. However, both methods are sensitive to the choice of basis set [5].

In the presence of a strong magnetic field, the wavefunction is heavily distorted along the field direction, breaking spatial and time-reversal symmetries. Consequently, the symmetry of the chosen basis set has a profound impact on the accuracy of the results. By using the neural network ansatz, VMC can be improved to avoid the dependence of basis set choice on account of it being a universal approximator, leading to Neural Network Variational Monte Carlo (NN-VMC) [5, 6].

In addition, NN-VMC enables us to solve the full time-independent Schrödinger equation, including the nuclear part of the Hamiltonian, numerically without any approximation, which is known to be a difficult task for traditional approaches.

1.3.2 Ground State Energy and Binding Energy

In this project, we are going to study the total ground state energy of hydrogen molecule with either the singlet ($^1\Sigma$) or triplet ($^3\Sigma$) electron spin configuration. The symbol Σ denotes that the orbital angular momentum quantum number $l = 0$. The binding energy can, hence, be calculated based on the energy difference between the hydrogen atom and molecule at various field strength. For fixed-nucleus systems, the optimal bond length retrieved from grid search, up the resolution of 0.01, will be used to run simulations. This information is not needed for quantum-nucleus cases. The configuration of hydrogen nuclei remains parallel to the magnetic field throughout all fixed-nucleus simulations, as this is considered the minimal energy configuration [4, 7].

1.3.3 Comparison of Bond Lengths

The bond length without Born-Oppenheimer approximation can be retried from the quantum-nucleus simulations without any assumption, and this value shall be compared to fixed nuclei bond lengths to verify the validity of Born-Oppenheimer approximation.

1.3.4 Validating the Method Against Analytical Models

Since the analytical solution for the hydrogen molecule is not available, the NN-VMC method must be validated against simpler models with known analytical or numerical results from traditional approaches. Here, we studied the two-electron magnetic system in harmonic potential and investigated its ground-state energy by numerically solving the differential equation. The numerical solutions at specific field strengths were then used to benchmark the accuracy of FermiNet at different field strengths. We also discuss a new non-columbic analytical model that can be used to benchmark the simulations for any number of Boltzmannons.

Methodology

2.1 Neural Network Variational Monte Carlo

2.1.1 Variational Monte Carlo

The framework of VMC relies on a fundamental principle, which is the variational principle of Quantum mechanics. Given a Hamiltonian operator $\hat{H}$, the minimal energy eigenvalue can be reached if and only if the trial wavefunction is exactly the ground state wavefunction. This statement writes mathematically

$$|\psi_{\text{ground}}\rangle = \arg\min_{|\psi\rangle \in \mathcal{L}^2} \frac{\langle\psi|\hat{H}|\psi\rangle}{\langle\psi|\psi\rangle}, \tag{2.1}$$

where $\mathcal{L}^2$ stands for the Hilbert space. Using the form of $\frac{\langle\psi|\hat{H}|\psi\rangle}{\langle\psi|\psi\rangle}$ does not require the function to be normalised. Converting this to a computable function can proceed as follows:

$$\frac{\langle\psi|\hat{H}|\psi\rangle}{\langle\psi|\psi\rangle} = \frac{\int d^3\vec{r}\ \langle\psi|\vec{r}\rangle\hat{H}\langle\vec{r}|\psi\rangle}{\int d^3\vec{r}\ \langle\psi|\vec{r}\rangle\langle\vec{r}|\psi\rangle} = \int d^3\vec{r} \left(\frac{|\psi(\vec{r}_i)|^2}{\int d^3\vec{r}\ |\psi(\vec{r}_i)|^2}\right) \frac{\hat{H}\psi(\vec{r}_i)}{\psi(\vec{r}_i)}. \tag{2.2}$$

Here $\psi(\vec{r}_i)$ denotes the multi-body wavefunction and the integral $\int d^3\vec{r}$ applies to the entire space. The part

$$\rho(\vec{r}_i) \equiv \frac{|\psi(\vec{r}_i)|^2}{\int d^3\vec{r}\ |\psi(\vec{r}_i)|^2}, \tag{2.3}$$

can be interpreted as a probability density function.

This integral is numerically computed by the Monte Carlo integration technique combined with importance sampling. Metropolis-Hasting sampling is the default choice for the sampling algorithm and is outlined in A.4. Consequently, the energy integral can be computed by talking the average over walkers, that is

$$\langle\hat{H}\rangle = \int d^3\vec{r}\ \rho(\vec{r}_i)\frac{\hat{H}\psi(\vec{r}_i)}{\psi(\vec{r}_i)} \approx \mathrm{E}_{\vec{r}_i\sim\rho(\vec{r}_i)}\left(\frac{\hat{H}\psi(\vec{r}_i)}{\psi(\vec{r}_i)}\right). \tag{2.4}$$

The wavefunction ansatz ψ is usually parametrised by some trainable parameters $\{\theta\}$ as $\psi_{\{\theta\}}$. For each walker update, the ansatz is optimised by some gradient-decent algorithm, naturally requiring a way to compute the gradient with respect to the parameters, which is given by

$$\nabla_{\{\theta\}}\langle\hat{H}\rangle = \mathrm{E}_{r_i\sim|\psi|^2}\left[\left(E_l\nabla_{\{\theta\}}\ln\psi^*_{\{\theta\}} + E_l^*\nabla_{\{\theta\}}\ln\psi_{\{\theta\}}\right) - 2\langle\hat{H}\rangle\nabla_{\{\theta\}}\ln|\psi_{\{\theta\}}|\right], \tag{2.5}$$

where the local energy E_l is defined as $E_l = \frac{\hat{H}\psi_{\{\theta\}}}{\psi_{\{\theta\}}}$ [5, 8]. This gradient equation is essential for complex wavefunctions, as required for magnetic systems. The Hamiltonian $\hat{H}$ indicated by Equation 1.10 was manually encoded in the program. The computed gradient can then be

passed to the optimisers, such as ADAM [9], for optimisation. Existing research suggested that the KFAC second-order optimiser [10] turned out to perform the best for our neural network ansatz [5].

2.1.2 Neural Network Ansatz

Due to Pauli exclusion principle, the wavefunction must be anti-symmetrical under the exchange of any two fermions of the same kind. The neural network ansatz architecture FermiNet is designed specifically for the NN-VMC framework. Traditional VMC uses ansatz based on slater determinants to enforce the anti-symmetry, which looks like

$$\Phi(\{r_i\}) = \underbrace{\begin{vmatrix} \phi_1(\vec{r}_1) & \phi_1(\vec{r}_2) & \phi_1(\vec{r}_3) & \cdots & \phi_1(\vec{r}_N) \\ \phi_2(\vec{r}_1) & \phi_2(\vec{r}_2) & \phi_2(\vec{r}_3) & \cdots & \phi_2(\vec{r}_N) \\ \vdots & \vdots & \vdots & \ddots & \vdots \\ \phi_{N-1}(\vec{r}_1) & \phi_{N-1}(\vec{r}_2) & \phi_{N-1}(\vec{r}_3) & \cdots & \phi_{N-1}(\vec{r}_N) \\ \phi_N(\vec{r}_1) & \phi_N(\vec{r}_2) & \phi_N(\vec{r}_3) & \cdots & \phi_N(\vec{r}_N) \end{vmatrix}}_{N \text{ columns}}. \tag{2.6}$$

Ferminet is constructed such that it gives many slater determinants and the final output can be taken as the sum of determinants. Each determinant looks like

$$\underbrace{\underbrace{\begin{vmatrix} \phi_1^{\uparrow}(\vec{r}_{1\uparrow};\{\vec{r}_{\setminus 1\uparrow}\}) & \cdots & \phi_1^{\uparrow}(\vec{r}_{N_\uparrow\uparrow};\{\vec{r}_{\setminus N_\uparrow\uparrow}\}) \\ \phi_2^{\uparrow}(\vec{r}_{1\uparrow};\{\vec{r}_{\setminus 1\uparrow}\}) & \cdots & \phi_2^{\uparrow}(\vec{r}_{N_\uparrow\uparrow};\{\vec{r}_{\setminus N_\uparrow\uparrow}\}) \\ \vdots & & \\ \phi_{N-1}^{\uparrow}(\vec{r}_{1\uparrow};\{\vec{r}_{\setminus 1\uparrow}\}) & \cdots & \phi_{N-1}^{\uparrow}(\vec{r}_{N_\uparrow\uparrow};\{\vec{r}_{\setminus N_\uparrow\uparrow}\}) \\ \phi_N^{\uparrow}(\vec{r}_{1\uparrow};\{\vec{r}_{\setminus 1\uparrow}\}) & \cdots & \phi_N^{\uparrow}(\vec{r}_{N_\uparrow\uparrow};\{\vec{r}_{\setminus N_\uparrow\uparrow}\}) \end{vmatrix}}_{N_\uparrow \text{ columns}} \underbrace{\begin{vmatrix} \phi_1^{\downarrow}(\vec{r}_{1\downarrow};\{\vec{r}_{\setminus 1\downarrow}\}) & \cdots & \phi_1^{\downarrow}(\vec{r}_{N_\downarrow\downarrow};\{\vec{r}_{\setminus N_\downarrow\downarrow}\}) \\ \phi_2^{\downarrow}(\vec{r}_{1\downarrow};\{\vec{r}_{\setminus 1\downarrow}\}) & \cdots & \phi_2^{\downarrow}(\vec{r}_{N_\downarrow\downarrow};\{\vec{r}_{\setminus N_\downarrow\downarrow}\}) \\ \vdots & & \\ \phi_{N-1}^{\downarrow}(\vec{r}_{1\downarrow};\{\vec{r}_{\setminus 1\downarrow}\}) & \cdots & \phi_{N-1}^{\downarrow}(\vec{r}_{N_\downarrow\downarrow};\{\vec{r}_{\setminus N_\downarrow\downarrow}\}) \\ \phi_N^{\downarrow}(\vec{r}_{1\downarrow};\{\vec{r}_{\setminus 1\downarrow}\}) & \cdots & \phi_N^{\downarrow}(\vec{r}_{N_\downarrow\downarrow};\{\vec{r}_{\setminus N_\downarrow\downarrow}\}) \end{vmatrix}}_{N_\downarrow \text{ columns}}}, \tag{2.7}$$

assuming these are $N_\uparrow$ electrons with up spin and $N_\downarrow$ with down spin. In equation 2.7, $\{\vec{r}_{\setminus i}\}$ denotes the position vectors excluding $\vec{r}$, and the parts of determinant for different spins use separate output channels and get concatenated together only at the very end. The order in $\{\vec{r}_{\setminus i}\}$ does not matter. Please refer to [5] and [11] for details.

The pre-determinantal part of FermiNet consists of an exponential envelope and a input-equivariant network. The envelope ensures that the wavefunction has a finite width and vanishes at infinity; the input-equivariant part enforces the wavefunction to obey the antisymmetry. Although the nuclear-electron and electron-electron cusp conditions were not encoded, experiments indicated that FermiNet was able to learn these conditions automatically while training [5].

In this study, the neural network was extended such that a unique determinant was generated for each type of Fermion, enabling us to study systems without Born-Oppenheimer approximation. FermiNet can be extended for Boltzmannonic systems by assigning independent output channels and columns in the determinants for each Boltzmannon [8].

2.1.3 Energies and Observables

Once the neural network is trained, the energy and desired observables can be calculated from the walkers and gradient information retried by the Metropolis-Hasting algorithm, without any optimisation step applied. This process is usually referred to as the "inference" run in machine learning contexts.

The observables of concern here were the particle densities and binding energies. As the wavefunction used in FermiNet was multi-particle in nature, it is generally considered impossible to visualise it directly. Therefore, the density plots were created by recording the walker positions during inference runs, equivalent to taking importance sampling for the multi-particle wavefunction, and plotting the corresponding multi-dimensional histogram. Binding energies were calculated by subtracting the sum of independent atomic hydrogen energies in magnetic fields from the total energy of hydrogen molecule systems.

In quantum-nucleus simulations, the equilibrium bond length was computed by taking the average of distances between the two nuclei among all walkers. This approach could be validated, as shown in later sections, by the fact that the distribution of bond lengths forms a bell-shaped curve.

The energies of hydrogen atoms were computed at various field strength with and without Born-Oppenheimer approximation for calculating the binding energy for fixed-nucleus and quantum-nucleus simulations, respectively.

2.1.4 Implementation and Validation

The Hamiltonian given by Equation 1.10 and the quantum-nucleus simulation framework were implemented independently and originally based on [8] by us. The installation was validated by retrieving the known ground state energy values of atomic and molecular hydrogen. All simulations were ran on one booster node with 1 or 4 A100 GPUs.

2.2 Analytical Models

2.2.1 Two-Electron System in a Harmonic Potential

The Hamiltonian of a two-electron system in a magnetic field and harmonic potential ω_0 is given by:

$$\hat{H} = \frac{(\vec{p}_1 + \vec{A}_1)^2}{2} + \frac{(\vec{p}_2 + \vec{A}_2)^2}{2} + \frac{1}{2}\omega_0^2 r_1^2 + \frac{1}{2}\omega_0^2 r_2^2 + \frac{1}{|\vec{r}_1 - \vec{r}_2|}, \tag{2.8}$$

commonly referred to as Hooke's atom. This system is typically solved by transforming to centre-of-mass (COM) and relative coordinates, defined as $\vec{r} = \vec{r}_2 - \vec{r}_1$ and $\vec{R} = \frac{1}{2}(\vec{r}_1 + \vec{r}_2)$, with corresponding momenta $\vec{p}_r = \frac{1}{2}(\vec{p}_2 - \vec{p}_1)$ and $\vec{p}_R = \vec{p}_1 + \vec{p}_2$. The associated vector potentials are $\vec{A}_r = \frac{1}{2}(\vec{A}_2 - \vec{A}_1) = \frac{1}{4}\vec{B} \times \vec{r}$ and $\vec{A}_R = \vec{A}_1 + \vec{A}_2 = \vec{B} \times \vec{R}$.

Substituting these transformations into the Hamiltonian, the system decouples into three components:

$$\hat{H} = \frac{1}{2}\hat{H}_R + 2\hat{H}_r + \hat{H}_s, \tag{2.9}$$

where:

$$\hat{H}_R = \frac{1}{2}\left[\frac{(\vec{p}_R + \vec{A}_R)^2}{2} + \frac{1}{2}\omega_R^2 R^2\right], \quad \text{with } \omega_R = 2\omega_0, \tag{2.10}$$

$$\hat{H}_r = 2\left[\frac{(\vec{p}_r + \vec{A}_r)^2}{2} + \frac{1}{2}\omega_r^2 r^2 + \frac{1}{2r}\right], \quad \text{with } \omega_r = \frac{\omega_0}{2}. \tag{2.11}$$

The total wavefunction and energy are expressed as:

$$\Psi = \varphi(r) \cdot \xi(\vec{R}) \cdot \chi(s_1, s_2), \quad E = 2\varepsilon_r + \frac{1}{2}\eta_R + E_{\text{spin}}. \tag{2.12}$$

Here, $\xi(\vec{R})$ solves the COM Hamiltonian $\hat{H}_R$ with energy η_R, which is equivalent to the Fock-Darwin Hamiltonian. The relative coordinate wavefunction $\varphi(r)$ corresponds to $\hat{H}_r$, yielding energy ε_r. Due to antisymmetric spins, the spin Hamiltonian contribution, E_{spin}, is disregarded.

For the ground state, where angular momentum is zero, the relative Hamiltonian reduces to the following radial equation with the ansatz $\varphi(r) = \frac{1}{\sqrt{2\pi}}\frac{u(r)}{r^{1/2}}$:

$$\left[-\frac{1}{2}\frac{d^2}{dr^2} - \frac{1}{8r^2} + \frac{1}{2}\tilde{\omega}_r^2 r^2 + \frac{1}{2r}\right] u(r) = \varepsilon_r u(r), \tag{2.13}$$

where $\tilde{\omega}_r = 2\tilde{\omega}$ and $\tilde{\omega} = \sqrt{\omega_0^2 + (B/2)^2}$ [12, 13].

2.2.2 N-Boltzmannons with Quadratic Interactions

To benchmark solutions for a system with N particles against an analytical model, we propose a quadratic repulsion model in a harmonic potential. The Hamiltonian is given by:

$$H = \sum_i \frac{1}{2}\left(p_i - A_i\right)^2 + \frac{1}{2}\sum_i k r_i^2 - \sum_{i,j}\frac{\alpha}{2}\left(r_i - r_j\right)^2, \tag{2.14}$$

where k is the spring constant for the harmonic potential, and α is the coefficient of the particle interaction. In this model, the harmonic potential and quadratic interaction terms can be combined into a single matrix $M_{i,j}$. Diagonalizing this matrix reduces the problem to a sum of Fock-Darwin equations, providing a compact expression for the ground-state energy:

$$E = 2\sqrt{k^2 + \frac{B^2}{4}} + 2(N-1)\sqrt{(-2\alpha N + k)^2 + \frac{B^2}{4}}. \tag{2.15}$$

This approach offers an analytical solution for the ground-state energy of the system. However, due to time constraints, we were unable to compare our simulations to this analytical model. This is an original model and for a full detailed derivation, refer to Appendix A.3. This method is limited, for now, to Boltzmannons. This is because after the coordinate transformation, the new coordinates are a function of previous coordinates of all the particles. This disallows us from being able to use a slater determinant for exchange symmetry and requires distinguishably.

Results & Discussion

3.1 Bond Lengths and Energies

3.1.1 Results

The bond length values retrieved from quantum-nucleus simulations, along with a comparison to the values obtained through a grid search with a resolution of 0.01 a.u. based on fixed-nucleus simulations, are presented in Table 3.1. The configuration of hydrogen nuclei remain parallel to the field for all fixed-nucleus simulations. Please note that the bond length in fixed-nucleus simulations is deterministic in nature and, therefore, does not possess uncertainty. However, the energy curves are very shallow, as shown by Figure 3.1, around the minima for triplet states, making it challenging to precisely determine the location of the minima. This results in an uncertainty in the bond length values for fixed-nucleus simulations for triplet states.

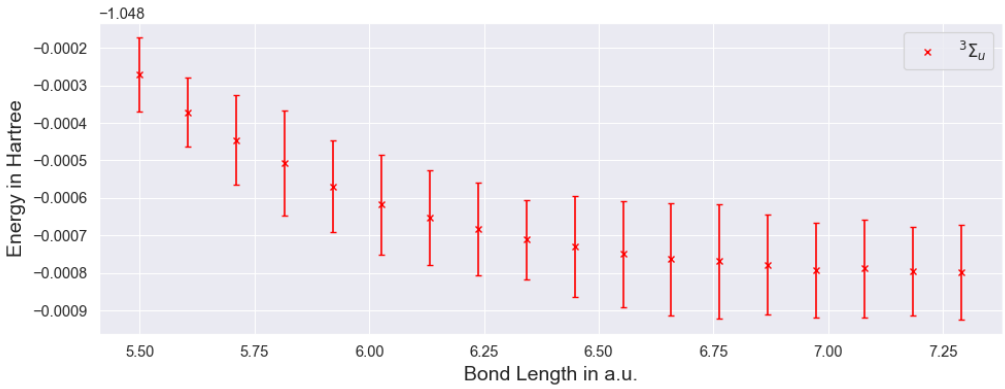

Figure 3.1: The energy versus bond length curve at $B = 0.05$ for triplet states is shown, with all values expressed in atomic units. The curve becomes flatter as the bond length increases but exhibits a very shallow minimum in the range of $7.2a_0$ to $7.9a_0$. The shape of the curve is consistent with the results reported in [7].

These uncertainties were estimated by repeating the grid search 10 times and identifying the range within which the minimum consistently occurs. Conducting additional grid searches to refine the uncertainties was not feasible due to time constraints.

The bond length observable forms bell-shaped distributions in quantum-nucleus simulations, as shown in Figure 3.2. A typical nuclei density map is also shown in the same figure, which has a cigar-like shape due to the distortion from the external magnetic field, in agreement with the theory.

The total and binding energy values of molecular hydrogen computed from both approaches are listed in Table 3.2 and 3.3 with comparison to existing CI-based results from [7], respectively. Please note the binding energy table was for singlet states only. We decided not to report the values for triplet states because the energy differences fall within the range of uncertainty and do not exhibit stable values.

All values presented in this section were the average values of 10000 steps inference run after 100000 steps of training. Please refer to A.5 for the network hyperparameters.

Triplet		Singlet		
Fixed Bond Length	Quantum Bond Length	Fixed Bond Length	Quantum Bond Length	Magnetic Field
7.89(2) [7.9]	5.19(84)	1.40 [1.40]	1.46(21)	0.001
7.89(2) [7.9]	5.23(86)	1.40 [1.40]	1.46(21)	0.005
7.88(2) [7.9]	5.18(83)	1.40 [1.40]	1.46(21)	0.01
7.88(2) [7.9]	4.99(78)	1.39 [1.40]	1.46(21)	0.05
7.83(2) [7.8]	4.87(78)	1.39 [1.39]	1.45(21)	0.1
7.67(3) [7.7]	4.72(79)	1.39 [1.39]	1.44(21)	0.2
7.44(3) [7.4]	4.58(95)	1.33 [1.33]	1.38(20)	0.5
7.46(2) [7.5]	4.23(82)	1.24 [1.24]	1.28(21)	1.0

Table 3.1: Bond length values retrieved from fixed- and quantum-nucleus simulations, up to 2 decimal places. The values in square brackets are the benchmark quoted from [7] based on an adapted CI method. All values presented in the table are in atomic units.

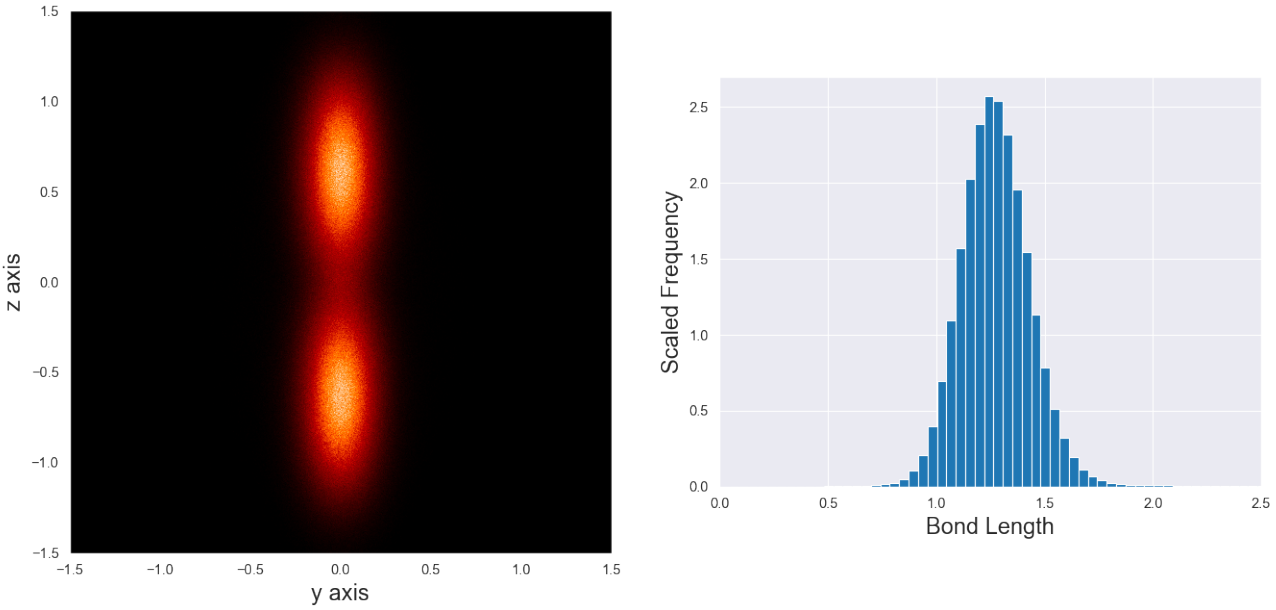

Figure 3.2: The x-y plane density map of nuclei in molecular hydrogen and the distribution of bond length values in a quantum-nucleus simulation at $B = 1$ a.u. with singlet spin configuration. The shape of atom was apparently distorted in the direction of external magnetic field (z direction).

3.1.2 Discussion

Interpreting the Results

For the singlet state in fixed-nucleus simulations, our VMC results are consistently lower than the values obtained using the conventional CI method by 0.05% to 0.1%, leading to higher binding energies. The energy values were shifted by approximately 0.1% of the total energy in all quantum-nucleus simulations compared to fixed-nucleus simulations at the same field strengths, due to the presence of nuclear kinetic and potential energies. This shift amounts to about 6% of the binding energy. The differences in bond length values are of the order of $0.5a_0$. Combined with the energy shifts, this suggests that the Born-Oppenheimer approximation causes significant deviations from the real scenario.

For the triplet states, the differences in total molecular energy between our results and those obtained from the conventional CI method become ambiguous and lie within the level of uncertainty. However, the change in bond length is significant, with a magnitude of $2a_0$.

Triplet		Singlet		
Total Energy - Quantum	Total Energy - Fixed	Total Energy - Quantum	Total Energy - Fixed	Magnetic Field
−0.99903(57)	−1.00099(15)[−1.00102]	−1.16362(41)	−1.17446(14)[−1.17344]	0.001
−1.00305(47)	−1.00498(16)[−1.00500]	−1.16356(37)	−1.17448(17)[−1.17342]	0.005
−1.00769(50)	−1.00993(18)[−1.00997]	−1.16350(43)	−1.17442(17)[−1.17340]	0.01
−1.04487(70)	−1.04880(14)[−1.04877]	−1.16172(39)	−1.17351(19)[−1.17241]	0.05
−1.08936(81)	−1.09516(12)[−1.09506]	−1.15718(44)	−1.17067(16)[−1.16965]	0.1
−1.17172(80)	−1.18097(18)[−1.18078]	−1.14272(51)	−1.15961(16)[−1.15877]	0.2
−1.37658(84)	−1.39494(21)[−1.39443]	−1.06294(47)	−1.08974(25)[−1.08908]	0.5
−1.63026(80)	−1.66334(24)[−1.66231]	−0.84795(55)	−0.89117(19)[−0.89034]	1.0

Table 3.2: Energy values retrieved from fixed- and quantum-nucleus simulations, up to 2 decimal places. The values in square brackets are the benchmark quoted from [7] based on an adapted CI method. All values are presented in atomic units.

Dissociated Energy - Quantum	Dissociated Energy - Fixed	Binding Energy - Quantum	Binding Energy - Fixed	Magnetic Field
−0.99859(40)	−1.00000(3)	0.16503(57)	0.17446(14)[0.17344]	0.001
−0.99864(46)	−0.99998(3)	0.16492(59)	0.17450(17)[0.17344]	0.005
−0.99851(42)	−0.99995(4)	0.16499(60)	0.17447(17)[0.17345]	0.01
−0.99623(26)	−0.99875(4)	0.16549(47)	0.17476(19)[0.17366]	0.05
−0.99078(28)	−0.99505(4)	0.15718(52)	0.17502(16)[0.17461]	0.1
−0.97292(54)	−0.98076(6)	0.16640(74)	0.17885(17)[0.17800]	0.2
−0.87698(50)	−0.89442(6)	0.18596(69)	0.19532(26)[0.19466]	0.5
−0.63020(69)	−0.66224(3)	0.21775(88)	0.22893(19)[0.22803]	1.0

Table 3.3: Energy values retrieved from fixed- and quantum-nucleus simulations, up to 2 decimal places, for the singlet state only. The values in square brackets are the benchmark quoted from [7] based on an adapted CI method. All values are presented in atomic units. The dissociated energy values were calculated as the energy sum of spin up and spin down hydrogen atoms.

Due to the Van der Waals attraction nature of the triplet binding state [7], existing research suggests that the binding energies are of the order of 1×10^{-5} Hartree [4, 7], which is at a level we are unable to resolve accurately with the current neural network setting.

Errors

The size of FermiNet was kept consistent across all fixed- and quantum-nucleus simulations for molecular hydrogen, respectively, which should, in principle, mitigate the systematic error efficiently. However, the network size was different for hydrogen atoms due to distinct system sizes and this might introduce a systematic bias for binding energy calculations. This could be mitigated by techniques like variance matching, but was not implemented due to the time constraint.

The convergence of VMC was checked by ensuring that the step-wise local energy variance fell below 10^{-8} Hartree. All calculations were conducted in 64-bit precision to minimise rounding errors. Random errors can be further reduced by increasing the inference run steps, at the cost of requiring more computational resources and time.

Limitation and Future Works

The uncertainty could be reduced by scaling up the neural network ansatz or introducing more efficient network architectures. This might enable us to accurately resolve the binding

energy for triplet states and surpass deterministic methods like CI, as in the case for singlet states. Some studies suggest that the Π states (i.e., $l = 1$) become the ground state as the field strength increases [4, 14]. This would require us to apply VMC to excited states, which is feasible following a recent study [15]. We shall leave these topics for future work.

3.2 Two-Electron System in Harmonic Potential

3.2.1 Results

Taut solved the relative Hamiltonian radial equation (equation 2.13) analytically for specific ω_r values using a terminated power series expansion. However, for ultra-high magnetic fields ($B \gg 1$), this method become impossible [12]. Here, we solve Equation (2.13) numerically using the finite difference method (FDM) with 2^{16} steps and Dirichlet boundary conditions ($u \to 0$ as $r \to 0$ and $u \to 0$ as $r \to 30$ a.u.). Details of this method are provided in Appendix A.2.

The numerical solutions show significant difference with Taut's semi-analytical results, with errors of approximately 1%. However, the numerical solution exhibits a cusp in $\varphi(r)$ and consequently in Ψ at $r = 0$, which is absent in Taut's solutions.

The energies retrieved from the FermiNet simulations and from the semi-analytical solutions are displayed in Figure 3.3a. The uncertainty margin of both the methods is extremely small and hence insignificant.

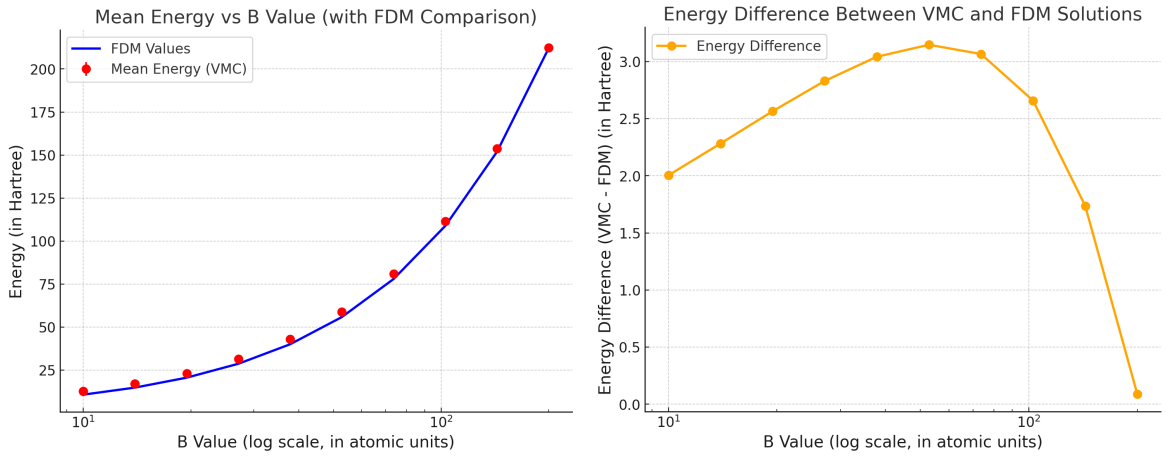

(a) FermiNet vs Finite Difference Method values

(b) Energy difference comparison

Figure 3.3: Comparison of energy between FermiNet and FDM solutions.

3.2.2 Discussion

On a relative scale, both FermiNet and the semi-analytical solution accurately capture the trend of increasing energy with increasing magnetic fields, attributed to the enhanced confinement potential. However, the observed disagreement between the two solutions, as shown in Figure 3.3, is unexpected, and its cause remains unclear. With two confining potentials in effect, a plausible explanation for the higher disagreement could be the increased complexity of the problem. Interestingly, the disagreement is minimal in the high magnetic field regime, where magnetic confinement significantly outweighs the influence of the harmonic potential.

Conclusion & Acknowledgement

4.1 Conclusion

This study explored the behaviour of molecular and atomic systems in ultra-strong magnetic fields using Neural Network Variational Monte Carlo (NN-VMC), focusing on the hydrogen molecule under varying field strengths. By conducting simulations with and without the Born-Oppenheimer approximation, we obtained ground-state energies for both singlet and triplet spin configurations. We also obtained the binding energy for the singlet state but couldn't do the same for the triplet state due to a shallow energy curve.

Key results from the study demonstrated that the NN-VMC method consistently achieved higher accuracy than conventional approaches like Configuration Interaction (CI). For the singlet state, our method provided energy values that were up to 0.1% lower than CI results, leading to a more precise determination of binding energies. Notably, the inclusion of nuclear motion in quantum-nucleus simulations revealed deviations from fixed-nucleus predictions, with bond lengths differing by approximately $0.5a_0$ for singlet states and up to $2a_0$ for triplet states. These findings emphasize the limitations of the Born-Oppenheimer approximation in strong magnetic fields and highlight the importance of coupling between nuclear motion and external fields.

In the benchmark study involving a two-electron system in a harmonic potential, NN-VMC results showed reasonable agreement with semi-analytical solutions. However, there was still a significant difference in the value outputted which still necessitates future work. We also proposed an analytical model to benchmark the NN-VMC simulations for an increasing number of particles.

This study demonstrates the potential of NN-VMC as a powerful computational tool for quantum systems under extreme conditions, offering new insights into the effects of ultra-strong magnetic fields on molecular and atomic behaviour.

4.2 Acknowledgement

We would like to thank Mr. Andres Perez Fadon for generously sharing his time with us to discuss topics in physics and giving very useful advices. Computer time was generously provided by our supervisor Prof. William Matthew Colwyn Foulkes at Cineca in Italy and JUWELS in Germany.

We acknowledge that ChatGPT (GPT4) was used to improve the logical flow and accuracy of this article.

Appendix

A.1 Cyclotrons, Landau Levels and Fock-Darwin States

The Schrödinger Equation for most magnetic systems cannot be solved exactly, with some exceptions. A single electron in the x-y plane in a z-directional uniform magnetic field is the simplest of its kind, referred to as the cyclotron model. Studying it could give us some insights into the standard behaviour of particles in a magnetic system and its characteristic scales. The Hamiltonian for this model writes

$$\hat{H} = \frac{1}{2m_e}\left(\hat{\vec{p}} + e\vec{A}\right)^2, \tag{A.1}$$

in standard SI units.

Suppose we define the mechanical momentum operator $\hat{\pi} = \hat{\vec{p}} + e\vec{A}$ and use the symmetric Coulomb gauge, the creation and annihilation operator may be defined as

$$a = \frac{1}{\sqrt{2e\hbar B}}(\pi_x - i\pi_y) \quad a^\dagger = \frac{1}{\sqrt{2e\hbar B}}(\pi_x + i\pi_y). \tag{A.2}$$

The Hamiltonian could be rewritten as

$$\hat{H} = \frac{1}{2m}(e\hbar B)(1 + 2a^\dagger a) = \hbar\frac{eB}{m}\left(\frac{1}{2} + a^\dagger a\right) \equiv \hbar\omega_c\left(\frac{1}{2} + a^\dagger a\right), \tag{A.3}$$

where the cyclotron frequency $\omega_c = \frac{eB}{m_e}$. Hence, the energy levels, referred to as the Landau levels, are

$$E = \hbar\omega_c\left(\frac{1}{2} + n\right), \; n \in \mathbb{Z}^+ \cup \{0\}. \tag{A.4}$$

The quantity $\hbar\omega_c$ sets the characteristic energy scale of the system. Following the dispersion $\omega = \frac{\hbar k^2}{2m_e}$, one can derive the length scale of the system

$$\rho_0 \sim k^{-1} \sim \sqrt{\frac{\hbar}{m_e\omega_c}} = \sqrt{\frac{\hbar}{eB}}, \tag{A.5}$$

which serves as the characteristic scale of the system, is referred to as the cyclotron radius.

In reality, magnetic systems often appear in confining potentials, naturally leading to the idea of adding a quadratic potential term to the Hamiltonian, which writes

$$\hat{H} = \frac{1}{2m_e}\left(\hat{\vec{p}} + e\vec{A}\right)^2 + \frac{1}{2}\omega_0^2\left(x^2 + y^2\right). \tag{A.6}$$

As the term $(x^2 + y^2)$ indicates, this is also a two-dimensional model. Fortunately this is also analytically solvable. The energy levels are given by

$$E = \hbar\Omega(2n + |l| + 1) + \frac{1}{2}\hbar\omega_c l, \tag{A.7}$$

where the modified frequency Ω is defined by $\Omega = \sqrt{\omega_0^2 + \frac{\omega_c^2}{4}}$. The associated energy eigenstates

are named Fock-Darwin states, which serves as a very useful analytical benchmark for real magnetic quantum systems. [16]

A.2 Finite Difference Method

The finite difference method works by discretizing space. It then solves the function by approximating the derivatives as differences between neighbouring grid-points. The second derivative using the central difference method is given by:

$$\frac{d^2y}{dx^2} \approx \frac{y_{i+1} - 2y_i + y_{i-1}}{\Delta x^2}. \tag{A.8}$$

Similarly, the first derivative is given by:

$$\frac{dy}{dx} \approx \frac{y_{i+1} - y_{i-1}}{2\Delta x}. \tag{A.9}$$

We can now represent, the differential equation needed to be solved:

$$\left\{-\frac{1}{2}\frac{d^2}{dr^2} - \frac{1}{8r^2} + \frac{1}{2}\tilde{\omega}_r^2 r^2 + \frac{1}{2r}\right\} u(r) = \varepsilon_r u(r), \tag{A.10}$$

with a tridiagonal matrix:

$$\begin{bmatrix} \gamma_1 & \beta_1 & 0 & 0 & \cdots & 0 \\ \alpha_1 & \gamma_2 & \beta_2 & 0 & \cdots & 0 \\ 0 & \alpha_2 & \gamma_3 & \beta_3 & \cdots & 0 \\ \vdots & \vdots & \vdots & \ddots & \vdots & \vdots \\ 0 & 0 & 0 & \cdots & \alpha_{N-1} & \gamma_N \end{bmatrix} \begin{bmatrix} u_1 \\ u_2 \\ \vdots \\ u_N \end{bmatrix} = E \begin{bmatrix} u_1 \\ u_2 \\ \vdots \\ u_N \end{bmatrix},$$

where:

$$\gamma_i = \frac{1}{\Delta r^2} + \frac{l^2 - 0.25}{2r_i^2} + \frac{1}{2}\omega_r^2 r_i^2,$$
$$\alpha_i = \beta_i = -\frac{1}{2\Delta r^2}.$$

The eigenvalues and eigenvectors of this matrix are then determined such that $Hu = Eu$ where u is a column matrix.

The above method already has the boundary conditions applied.This is because this method assumes the contribution u_0 on the evaluation of $u1$ is 0. Similarly the boundary condition for u_{N+1} is also applied.

A.3 N - Boltzmannons with Quadratic Interactions

The interaction of n Boltzmannons at positions r_i in a magnetic field with gauge $A = \frac{1}{2}\vec{B} \times \vec{r}$ with non-coulombic quadratic attraction in a harmonic potential is given by:

$$H = (p_{i,\beta} - A_{i,\beta})(p_{i,\beta} - A_{i,\beta}) + \frac{1}{2}kr_{i,\beta}r_{i,\beta} - \sum_{i,j}^{n} \frac{\alpha}{2}(r_{i,\beta} - r_{j,\beta})(r_{i,\beta} - r_{j,\beta}). \tag{A.11}$$

The term 1/2 in front of α exists simply because every interaction is being added twice in the potential function. β here is the component of the coordinate and the indices i, j denote the particles.

The position coordinates can be expanded as:

$$(r_{i,\beta} - r_{j,\beta})(r_{i,\beta} - r_{j,\beta}) = r_{i,\beta}r_{i,\beta} + r_{j,\beta}r_{j,\beta} - r_{i,\beta}r_{j,\beta} - r_{j,\beta}r_{i,\beta}. \tag{A.12}$$

Inspecting Equation A.12, each cross-index correlation appears twice in the mesh of all i and j iterations, while each same-index correlation corresponds to the number of ways to choose 2 indices from the n total indices, multiplied by 2 to account for two terms being present above. We, therefore, represent the potential with the below form:

$$\frac{1}{2}kr_{i,\beta}r_{i,\beta} - \sum_{i,j}^{n} \frac{\alpha}{2}(r_{i,\beta} - r_{j,\beta})(r_{i,\beta} - r_{j,\beta}) = \frac{1}{2}M_{i,j}r_{i,\beta}r_{j,\beta} \tag{A.13}$$

where

$$M_{ij} = \begin{cases} -2\alpha\binom{n}{2} + k & \text{if } i = j, \\ 2\alpha & \text{if } i \neq j. \end{cases} \tag{A.14}$$

This gives us the following form of the equation:

$$H = (p_{i,\beta} - A_{i,\beta})(p_{i,\beta} - A_{i,\beta}) + \frac{1}{2}r_{i,\beta}M_{i,j}r_{j,\beta}. \tag{A.15}$$

Now, we find a transformation of basis O such that $(O^T)_{i,j}O_{i,j} = I$ and $(O^T)_{i,k}m_kO_{j,k} = M_{i,j}$ where m_k is a diagonal matrix with indices k, containing the eigenvalues of M. Applying this O transformation on all matrices as below:

$$H = (p_{i,\beta} - A_{i,\beta})(O^T)_{i,k}O_{i,k}(p_{i,\beta} - A_{i,\beta}) + \frac{1}{2}r_{i,\beta}(O^T)_{i,k}m_kO_{j,k}r_{j,\beta}. \tag{A.16}$$

We treat the above Hamiltonian as:

$$H = \sum_{k}^{n} H_k \tag{A.17}$$

with

$$H_k = \sum_{\beta} |(p_{\beta,k} - A_\beta(r_k)|^2 + \frac{1}{2}m_k|r_{k,\beta}|^2. \tag{A.18}$$

Again, note that the observables haven't changed in this equation, only the basis vectors have. This means that all the above quantities have remained unchanged but we have diagonalized the matrix.

Since we are only concerned with the ground state and angular momentum $l = 0$, H has the following solution:

$$E = \sum E_k = \sum \left(m_k^2 + \frac{B^2}{4}\right)^{1/2}.$$

With matrix manipulations of M, we get the solution:

$$E = 2\sqrt{k^2 + \frac{B^2}{4}} + 2(N-1)\sqrt{(-2\alpha N + k)^2 + \frac{B^2}{4}}. \tag{A.19}$$

A.4 Metropolis-Hasting Algorithm

Metropolis-Hasting sampling, as explained in Algorithm 1, is the default choice for the sampling algorithm. The sampled positions of a set of particles are collectively referred to as a walker. Please note the batch dimension B is ignore in Algorithm 1 for the sake of simplicity.

Algorithm 1 Metropolis-Hasting Sampling for VMC with N particles

Input: current walker position $r_i \in \mathbb{R}^{3N}$, mapping $\psi : \mathbb{R}^{3N} \mapsto \mathbb{R}$, step size $s \in \mathbb{R}^N$
procedure METROPOLIS-HASTING(r_i, ψ, s)
    $r_i' \leftarrow r_i + s\epsilon_i,\ \epsilon_i \sim \mathcal{N}(0,1)$ ▷ propose new position by adding a Gaussian noise
    if $|\psi(r_i')|^2/|\psi(r_i)|^2 \geq 1$ **then**
        $r_i \leftarrow r_i'$
    else
        if $|\psi(r_i')|^2/|\psi(r_i)|^2 > k,\ k \sim \text{uniform}(0,1)$ **then** ▷ draw a random threshold
            $r_i \leftarrow r_i'$
        else
            pass
        end if
    end if
    return r_i ▷ Output: the updated walker position
end procedure

A.5 Hyperparameters for FermiNet

Parameter	Value
batch_size	4096
optim.iterations	100000
optim.laplacian	'folx'
optim.lr.rate	0.05
network.network_type	'ferminet'
network.determinants	32
mcmc.burn_in	0
log.walkers	True
log.walkers_log_frequency	1
network.complex	True

Table A.1: Configuration Parameters

Bibliography

[1] Stella Stopkowicz. "Perspective: Coupled cluster theory for atoms and molecules in strong magnetic fields". In: *International Journal of Quantum Chemistry* 118.1 (2018), e25391. DOI: 10.1002/qua.25391. URL: https://onlinelibrary.wiley.com/doi/10.1002/qua.25391.

[2] P. Schmelcher and L. S. Cederbaum. "Molecules in strong magnetic fields: Some perspectives and general aspects". In: *International Journal of Quantum Chemistry* 64.5 (1997), pp. 501–511. DOI: https://doi.org/10.1002/(SICI)1097-461X(1997)64:5<501::AID-QUA3>3.0.CO;2-\#. eprint: https://onlinelibrary.wiley.com/doi/pdf/10.1002/%28SICI%291097-461X%281997%2964%3A5%3C501%3A%3AAID-QUA3%3E3.0.CO%3B2-%23. URL: https://onlinelibrary.wiley.com/doi/abs/10.1002/%28SICI%291097-461X%281997%2964%3A5%3C501%3A%3AAID-QUA3%3E3.0.CO%3B2-%23.

[3] P. Schmelcher, L. S. Cederbaum, and H.-D. Meyer. "Electronic and nuclear motion and their couplings in the presence of a magnetic field". In: *Phys. Rev. A* 38 (12 1988), pp. 6066–6079. DOI: 10.1103/PhysRevA.38.6066. URL: https://link.aps.org/doi/10.1103/PhysRevA.38.6066.

[4] Dong Lai. "Matter in strong magnetic fields". In: *Rev. Mod. Phys.* 73 (3 2001), pp. 629–662. DOI: 10.1103/RevModPhys.73.629. URL: https://link.aps.org/doi/10.1103/RevModPhys.73.629.

[5] David Pfau et al. "Ab initio solution of the many-electron Schrödinger equation with deep neural networks". In: *Phys. Rev. Res.* 2 (3 2020), p. 033429. DOI: 10.1103/PhysRevResearch.2.033429. URL: https://link.aps.org/doi/10.1103/PhysRevResearch.2.033429.

[6] Hannah Lange et al. *From Architectures to Applications: A Review of Neural Quantum States*. 2024. arXiv: 2402.09402 [cond-mat.dis-nn]. URL: https://arxiv.org/abs/2402.09402.

[7] T. Detmer et al. "Hydrogen molecule in magnetic fields: The ground states of the Σ manifold of the parallel configuration". In: *Phys. Rev. A* 56 (3 1997), pp. 1825–1838. DOI: 10.1103/PhysRevA.56.1825. URL: https://link.aps.org/doi/10.1103/PhysRevA.56.1825.

[8] David Pfau James S. Spencer and FermiNet Contributors. *FermiNet*. 2020. URL: http://github.com/deepmind/ferminet.

[9] Diederik P. Kingma and Jimmy Ba. *Adam: A Method for Stochastic Optimization*. 2017. arXiv: 1412.6980 [cs.LG]. URL: https://arxiv.org/abs/1412.6980.

[10] James Martens and Roger Grosse. *Optimizing Neural Networks with Kronecker-factored Approximate Curvature*. 2020. arXiv: 1503.05671 [cs.LG]. URL: https://arxiv.org/abs/1503.05671.

[11] Ingrid von Glehn, James S. Spencer, and David Pfau. *A Self-Attention Ansatz for Ab-initio Quantum Chemistry*. 2023. arXiv: 2211.13672 [physics.chem-ph]. URL: https://arxiv.org/abs/2211.13672.

[12] M Taut. "Two electrons in a homogeneous magnetic field: particular analytical solutions". In: *Journal of Physics A: Mathematical and General* 27.3 (1994), pp. 1045–1055. DOI: 10.1088/0305-4470/27/3/040.

[13] W.M.C. Foulkes. *Two-Dimensional Hooke's Atom in a Magnetic Field*. Tech. rep. Based on M. Taut, J. Phys. A: Math. Gen. 27, 1045 (1994). Department of Physics, Imperial College London, 2024.

[14] T. Detmer, P. Schmelcher, and L. S. Cederbaum. "Hydrogen molecule in a magnetic field: The lowest states of the Π manifold and the global ground state of the parallel configuration". In: *Phys. Rev. A* 57 (3 1998), pp. 1767–1777. DOI: 10.1103/PhysRevA.57.1767. URL: https://link.aps.org/doi/10.1103/PhysRevA.57.1767.

[15] David Pfau et al. "Accurate computation of quantum excited states with neural networks". In: *Science* 385.6711 (Aug. 2024). ISSN: 1095-9203. DOI: 10.1126/science.adn0137. URL: http://dx.doi.org/10.1126/science.adn0137.

[16] V. Fock. "Bemerkung zur Quantelung des harmonischen Oszillators im Magnetfeld". In: *Zeitschrift für Physik* 47.5 (1928), pp. 446–448. ISSN: 0044-3328. DOI: 10.1007/BF01390750. URL: https://doi.org/10.1007/BF01390750.